Chapter 4

Doping Effects of Pigment Oxides on Optical and Mechanical Properties of PbO-Based Glasses

4.1 Introduction

The most commonly available commercial glasses are silicates, which have a high viscosity and enable glass formation without crystallization [99]. Many types of silicate glasses are used in construction, the decorative industry, electronics, radioactive and photovoltaic tools, acoustic-optic devices, and more because of their exceptional thermal resilience, thermo-mechanical qualities, and chemical-based strength [23,100]. They are also used in telecommunications optics because of their excellent transmission and low attenuation losses in the apparent and near-IR zones [101]. Due to its exceptional capacity to capture and transmit visible daylight into buildings, silicate glasses are increasingly found in both residential and commercial settings [102]. When compared to other building coverings, pure silicate glass produces notably clear glass with high transmission qualities. As a result, it becomes the primary source of additional solar radiation within the building, which makes the occupants of the building uncomfortable. This issue has been resolved, though, by doping silicate glasses with particular concentrations of transition metals or rare earth ions, which tints and absorbs heat without weakening the glasses, which lowers and regulates the considerable amount of solar radiation that enters buildings.

Regarding transition metals, copper's valence configuration in glasses affects not only the material's physical and chemical properties but also its capacity to form glasses [12]. According to ligand field theory, the presence of Cu^{2+} ions results in the production of the remarkable, dazzling, piercing blue-green color glass [13]. The electronic configuration of the copper atom is [Ar] $3d^{10}4s^{1}$, which includes the two persistent ion states Cu^{+} and Cu^{2+}. Because the five d-orbital of cuprous ion (Cu^{+}) is completely occupied, it does not provide color [14]. However, the Cu^{2+} ion

produces a color center with absorption bands in the visible-light region and gives materials an intriguing bluish, sometimes green, color [15]. The degree of coloring has been investigated in terms of the concentration of Cu^{2+} and its coordination, and the alkalinity of glasses has been included [14,15]. Cu^{2+} ion-doped glasses are currently the most researched topic because of their optical bistability [13,103]. In addition to doping with rare earth ions or transition metals, the glasses become more beneficial when appropriate amounts of heavy metallic oxides are added. Heavy metal oxides (BaO, Bi_2O_3, PbO, etc.) have been found to enhance some special qualities of glasses, including density, refractive index, and chemical resilience, as well as to improve resistance to devitrification and lower processing temperatures [16]. Additionally, the heavy metal oxide silicate glasses exhibit outstanding shielding capabilities against nuclear radiation and high mass attenuation coefficient values [17,104]. Numerous earlier studies noted that silicate glasses with appropriate concentrations of heavy metal oxides exhibited low crystallization propensity, superior infrared transmission, and improved linear and nonlinear optical characteristics [18-20]. Since these PbO-containing multicomponent glasses have low processing temperatures, high resistance to devitrification, high chemical durability, high optical density, and refractive index, they are widely used in enamels, optics (including lenses), ultrasonic delay cables, electro-optic modulators, electro-optic toggles, solid-state laser resources, electron boosts, television image tubes, and other related important optical electronic uses and glass-to-metal sealing [21-23]. Other scientific applications for such glasses include upconverting phosphors, mechatronics, dosimetry, radiation physics, and light waveguides due to their low phonon energy [105,106]. They can also be used in a particular field for mechanical and heated detectors, low-loss fiber optics, and infrared-transmitting components [107]. Pb^{2+}'s molecular significance in silica glass is now being

extensively studied to demonstrate its intriguing role during glass formation in a variety of forms, particularly silicon dioxide [**24**, **108**-**115**].

Previous authors have shown that Pb acts as both an interconnecting enhancer for a small amount of lead and a glassmaker with a substantial amount of lead in binary lead silicate glasses [**18**]. Although PbO cannot form a glass matrix by itself, it can make glass and build an ionic or covalent link between oxygen atoms when combined in appropriate proportions with other glass-forming oxides such as SiO_2, B_2O_3, TeO_2, and P_2O_5 [**25**,**116**]. In addition to transition metal ions and heavy metal oxides, it has been discovered that adding appropriate proportions of SnO_2 to the silicate glass structure enhanced the tinted glass's compactness, greatly facilitating the usage of the glass composition against high photon energy [**26**]. Prior studies also observed that the proper doping of SnO_2 in their glass composition improved the thermal stability, microhardness, and photosensitivity of the glass [**66**, **117**]. Ziemath et al. used the UV-visible absorbance & scattered reflection analysis in the infrared spectrum to assert that the Sn4+cations in their glass composition functioned as an interconnected former, resulting in more rigid glass formation [**27**]. Due to its restricted solubility inside the silica network, SnO_2 has the drawback of making silicate glass opacic at higher concentrations, which is undesirable when the glass is utilized as a building material [**28**]. However, the literature review above demonstrates that adding a small and regulated quantity of Sn^{4+}, Cu^{2+}, Cu^{+}, and Pb^{2+} ions to a soda silicate glass enhances its qualities, making it potentially appropriate for wider applications in a variety of disciplines. The creation of PbO-based tint glasses with enhanced optical and mechanical qualities for broad applications was the main emphasis of this research project, which was inspired by the literature review mentioned above. The optimization of PbO contents in tint glass compositions for optimal mechanical, optical, and physical qualities for building construction materials was also the other evident goal. Glass

interconnection structures were investigated using a variety of characterization approaches. These structures may be causally related to the enhanced mechanical, optical, optoelectronic, and physical characteristics of the tint glasses under investigation. Glass interconnection structures were investigated using a variety of characterization approaches. These structures may be causally related to the enhanced mechanical, optical, optoelectronic, and physical characteristics of the tint glasses under investigation.

4.2 Methods used in experiments

4.2.1 *Process of Making Tinted Glasses*

A variety of tint glass compositions were prepared using a sodium silicate base glass ($30Na_2O$-$70SiO_2$), and the related compositions are listed in **Table 4.1**. For all prepared compositions, the general formula is $xPbO\text{-}y(0.14Cu_2O\text{-}0.05CuO\text{-}0.03SnO_2)\text{-}30Na_2O\text{-}(70\text{-}0.22y\text{-}x)SiO_2$(x = 0,1.5,10 mol% and y = 0,1). High-purity reagent grade cuprous oxide (Cu_2O, 97% freshness), copper monoxide (CuO, 97% purity) supplied through Avarice Industries, and lead oxide (PbO, 99.99% purity) supplied by Aldrich Chemical Co. were employed as sources of Cu_2O, CuO, and PbO, respectively. High-purity reagent grade cuprous oxide (Cu_2O, 97% purity), copper monoxide (CuO, 97% purity) supplied through Avarice Industries, and lead oxide (PbO, 99.99% purity) supplied by Aldrich Chemical Co. were employed as sources of Cu_2O, CuO, and PbO, respectively. SnO_2, Na_2O, and SiO_2 were obtained using Loba Chemie-supplied quartz (SiO_2, 99% purity), sodium carbonate (Na_2CO_3, 99% purity), and tin oxide (SnO_2, 98% purity), respectively. An electronic micro-analytical weighing machine with a precision of ± 0.0001 g was used to weigh each batch composition. A high-powered ball mill (Amaze Instruments) was then used to blend the mixture at 400 rpm for two hours to create a homogenous batch. According to the melting profile displayed in **Fig. 4.1(a)**, each batch mixture was placed in an aluminum crucible

for glass melting in an electric furnace set at roughly 1400 °C for six hours. To create a more consistent glass formation, the molten glass was poured over a hot alumina plate, then chilled, ground, and then remelted with a comparable time-temperature profile. Finally, a heated iron mold with precise measurements for creating rectangular samples was filled with the remelted glass. To stop them from breaking because of internal residual stresses, the prepared rectangular fragments were annealed at 500 °C for 4 hours using a constant time-temperature profile, as shown in **Fig. 4.1(b)**.

Table 4.1. Molar compositions of the synthesized glasses along with their corresponding batch compositions (wt.%).

Glass samples	Molar glass compositions	Batch compositions (wt.%)					
		Cu_2O	CuO	SnO_2	PbO	Na_2O	SiO_2
Base Glass	$(Na_2O)_{30}(SiO_2)_{70}$	-	-	-	-	30.70	69.30
S1	$(PbO)_{1.50}(Na_2O)_{30}(SiO_2)_{68.50}$	-	-	-	5.31	29.50	65.19
S2	$(PbO)_{10}(Na_2O)_{30}(SiO_2)_{60}$	-	-	-	29.01	24.18	46.80
S3	$(Cu_2O)_{0.14}(CuO)_{0.05}(SnO_2)_{0.03}(Na_2O)_{30}(SiO_2)_{69.78}$	0.329	0.0654	0.074	-	30.61	68.91
S4	$(Cu_2O)_{0.14}(CuO)_{0.05}(SnO_2)_{0.03}(PbO)_{1.50}(Na_2O)_{30}(SiO_2)_{68.28}$	0.316	0.0628	0.071	5.29	29.42	64.82
S5	$(Cu_2O)_{0.14}(CuO)_{0.05}(SnO_2)_{0.03}(PbO)_{10}(Na_2O)_{30}(SiO_2)_{59.78}$	0.259	0.0515	0.058	28.95	24.132	46.53

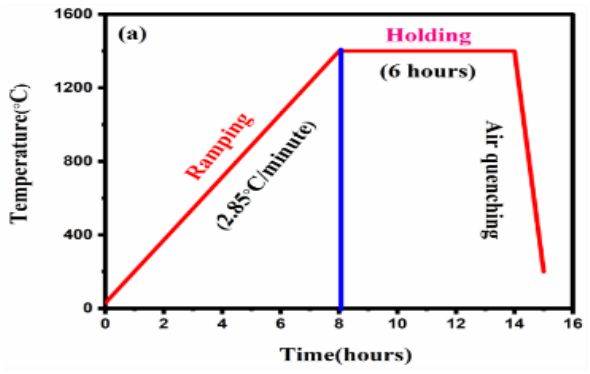

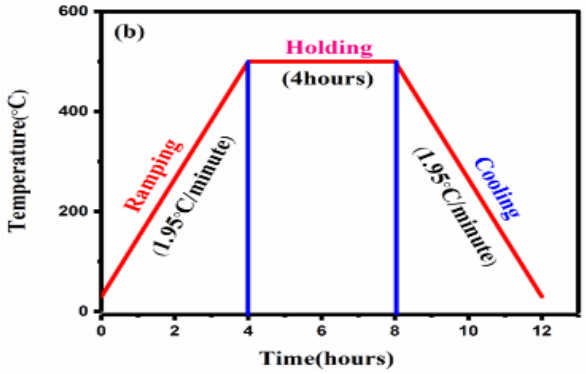

Fig. 4.1. (a) Time-temperature curve for the melt-quenching process, and (b) time-temperature curve for the annealing process.

4.2.2 *Characterization of Materials*

By using the law of Archimedes and water as the dipping liquid, the density of the manufactured tint glasses was determined at room temperature. The estimated variance of the entire density evaluation was around ± 0.004 g cm^{-3}. The molar volume of the prepared glasses was calculated using the formula $V_m = M/\rho$, where M is the molar mass, ρ is the glass density, and V_m is the molar volume. The formula $OPD = (1000 \times k \times \rho)/M$ was used to determine the oxygen packing density (OPD) of the glass specimens. In this calculation, k represents the number of oxygen atoms per mole in a composition, ρ represents the glass's density, and M represents the glass's molecular weight [**118**]. Each bulk glass sample was mechanically cut with a water-cooled low-speed diamond saw after being shaped and polished using 400/800/1200 water-cooled silicon carbide (SiC) dust and 6/3/1/0.025 µm diamond paste. Every effort was made to ensure that the sample surfaces were as flat as possible and that each side was aligned with the others with a fluctuation of less than 0.05 cm. **Fig. 4.2** displays the photos of the polished glass samples for optical characterization. The ultraviolet and visible spectrum of the optically polished glasses were recorded using a Jasco V-770 double-beam UV-VIS spectrophotometer (Japan) connected with PC UV-Win lab software. A weighted average of the experimental data of this spectrum over 360 nm to 830 nm was used to determine the visible and solar optical characteristics of the pigmented glasses. The weighted average of the experimental data of this spectrum over 360 nm to 830 nm was used to determine the pigmented glasses' visible and solar optical characteristics. The data was collected at 5-nm intervals while considering the normal incidence of light in the visible and ultraviolet spectral zones, which include absorption in the spectrum mode, transmission in the specular transmission mode, and reflection in the diffuse reflection mode. The US standard

atmosphere, which typically has 3.4 mm of ozone and 20 mm of precipitable H_2O vapor, was used to measure the weighted parameters for assessing solar optical properties [37]. The materials absorption coefficient $\alpha(\omega)$ for each glass at various photon energies $\hbar(\omega)$ was determined using the Lambert-Bear equation, $\left(I_t = I_0 e^{-\alpha(\omega)d}\right)$, where d is the sample thickness and I_0 and I_t are the incident and transmitted photon intensities, respectively. Using a mortar and pestle, all the prepared tint glasses were ground into fine powders to perform an XRD study at ambient temperature. The fine powder was collected in a sample holder at the 9 KW Ragaku Smart Lab powder-type X-ray diffraction apparatus of the RIGAKU Corporation firm (Japan). It was outfitted with a Ni filter tube operating at 40 kV and 20 mA current and a graphite monochromatic copper Kα radiation source ($\boldsymbol{\lambda}$ = 1.540 Å). Using a scan rate of 3º min^{-1}, all XRD data were acquired throughout a 2θ range from 10º to 80º. PANalytical XPert High Score was used to evaluate each data set, and standard ICDD (International Centre for Diffraction Data) cards were used for correlation. All the glass powder samples' infrared spectra were examined in transmittance mode at 4 cm^{-1} resolution throughout wavenumbers (4000-450 cm^{-1}) to highlight the functional groups present in the glasses. At room temperature, all the data were collected using the KBr disc technique on a single-beam Nicolet iS5 FTIR spectrometer manufactured by THERMO Electron Scientific Instruments LLC Company (USA). To compute the longitudinal (V_L) and shear (V_S) ultrasonic wave velocities of prepared glass samples at room temperature, an ultrasonic flaw detector machine was used. It has two quartz X- and Y-cut transducers operating at a resonant frequency of 5 MHz with an error of ± 10 m/s ambiguity.

4.3 Results and discussion

4.3.1 *Physical Characteristics of the Tinted Glasses*

It has been discovered that every glass that is made is transparent. In the respective oxide glass systems, {xPbO-y(0.14Cu_2O-0.05CuO-0.03SnO_2) -30Na_2O-(70-0.22y-x) SiO_2} authors indicated the composition of glass systems y(0) and y(1) when y=0 and y=1 respectively in

Fig. 4.2. Images of optically polished glass samples prepared for optical analysis are shown, where sample S1 has dimensions of 20.35 mm in length, 17.68 mm in breadth, and 7.96 mm in width; S2 measures 23.91 mm in length, 22.01 mm in breadth, and 8.10 mm in width; S3 has dimensions of 20.51 mm in length, 20.26 mm in breadth, and 8.01 mm in width; S4 measures 26.24 mm in length, 26.05 mm in breadth, and 8.06 mm in width; and S5 has dimensions of 18.50 mm in length, 17.17 mm in breadth, and 8.02 mm in width.

the corresponding glass composition. One important parameter that evaluates the stiffness of the oxide system and characterizes the glass structure is OPD. The OPD values of all the generated glass samples fall between 57.331 and 71.86 mol/liter. **Table 4.2** shows the density, molar volume, and OPD values. The data reveal that in sodium silicate glass systems, the addition of metallic oxides (<0.22mol%) (Cu_2O+CuO+SnO_2) and rising PbO concentrations ($0 \leq x \leq 10$, x in mol%) reduce OPD, which indicates the growth of NBOs in the glass latticework, leading to a more loosely packed network structure.

4.3.2 *Analysis of XRD*

Fig. 4.3 shows the XRD spectra of base glass and manufactured glass samples with various compositions reported in **Table 4.1**. The XRD data of all glass samples show a prominent initial

hump due to the base glass, as reported in a previous research paper [70]. The spectra covering the region of 2θ, 10° to 80° of all glass samples show no distinct peaks, indicating the irregular character of entire synthesized glass specimens due to the decided trace amount of doped ingredients.

Table 4.2. Density, molar volume, and oxygen packing density of the synthesized colored glasses.

Samples	Thickness (cm)	Density (g/cm^3)	Molar volume (cm^3/mol.)	Oxygen packing density (OPD)
S1	**0.796**	**2.689**	**23.446**	**71.86**
S2	**0.81**	**3.190**	**24.113**	**66.35**
S3	**0.801**	**2.491**	**24.389**	**69.63**
S4	**0.806**	**2.5856**	**22.471**	**68.85**
S5	**0.802**	**2.765**	**27.874**	**57.33**

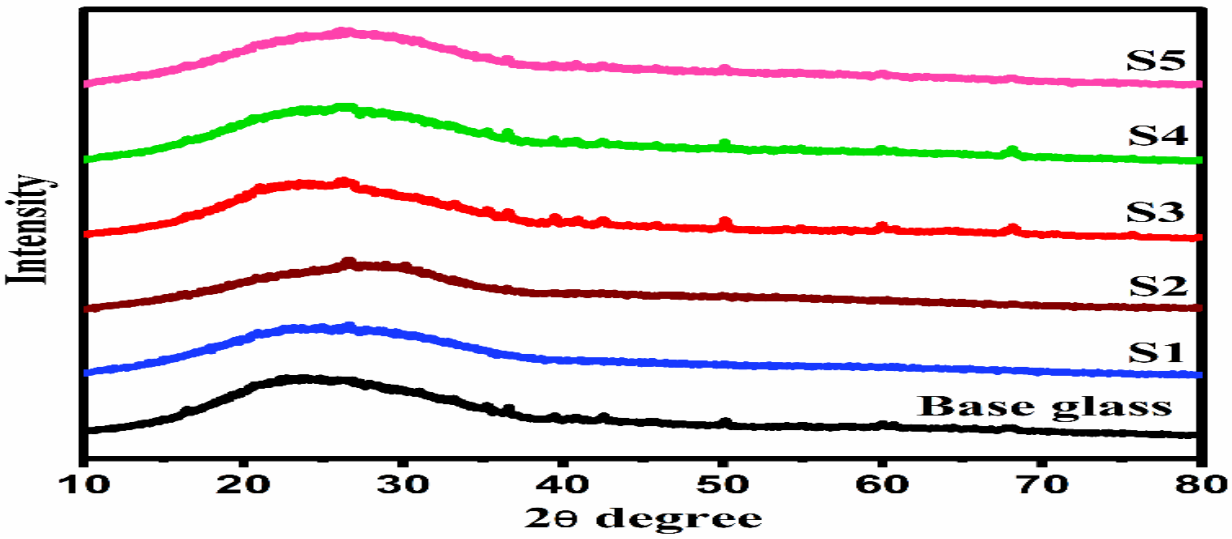

Fig. 4.3. XRD patterns of all synthesized glass samples.

4.3.3 *FTIR Analysis*

Fig. 4.4 shows the FTIR spectrum observations of base glass and all doped tint glasses with various compositions listed in **Table 4.1**. There are two distinct regions in the 500–4000 cm^{-1} range of the infrared spectrum. Although the functional group area, which appeared in the larger spectral region, is essential for determining the sample's basic properties, the characteristic vibrational bands, the bulk of which are situated in the smaller spectral region assigned to the IR spectral fingerprint region. A deep infrared wideband is visible at about 1038 cm^{-1}, two small dim infrared bands are found at around 1384 cm^{-1} & 1625 cm^{-1}, a strong infrared wideband is viewed at approximately 3440 cm^{-1}, and two moderately clear infrared bands form around 460 cm^{-1} & 783 cm^{-1}, respectively. The Si-O bond's uneven stretching vibration in the SiO_4 tetrahedron groups found in the glass samples' silicate phases caused the broad broadband at about 1038 cm^{-1} to appear in all the glass samples' FTIR spectra [**63**,**119**]. Due to the bending vibrations of the O-Si-O bond in the SiO_4 tetrahedron groups present in the glass samples and the vibrations of metallic cations like Pb^{2+}, another relatively wide band at around 460 cm^{-1} is obtained in all the FTIR glass sample data [**25**,**120**]. **Table 4.3** lists all the transmission peaks' ascribed assignments across all glass samples' FTIR data sets. Since all the FTIR glass sample data show no discernible changes, it can be said that the silicate network structure has not been significantly impacted by the measured concentrations of PbO and Cu_2O+CuO+SnO_2.

4.3.4 *UV-Visible Spectroscopy*

Fig. 4.5 displays the spectral transmission and reflection in the visible region as well as the absorbance in the ultraviolet and visible areas of the corresponding rectangular optically polished glass samples (S1, S2, S3, S4, and S5) with thicknesses ranging from 7.96 to 8.10 mm and varying compositions (**Table 4.1**). The colored glass samples S1, S2, S3, S4, and S5 all had measured

reflections that show their maximum intensity band in the visible range at approximately 830 nm, 528 nm, 528 nm, 497 nm, and 484 nm, respectively (**Fig. 4.5(a)**).

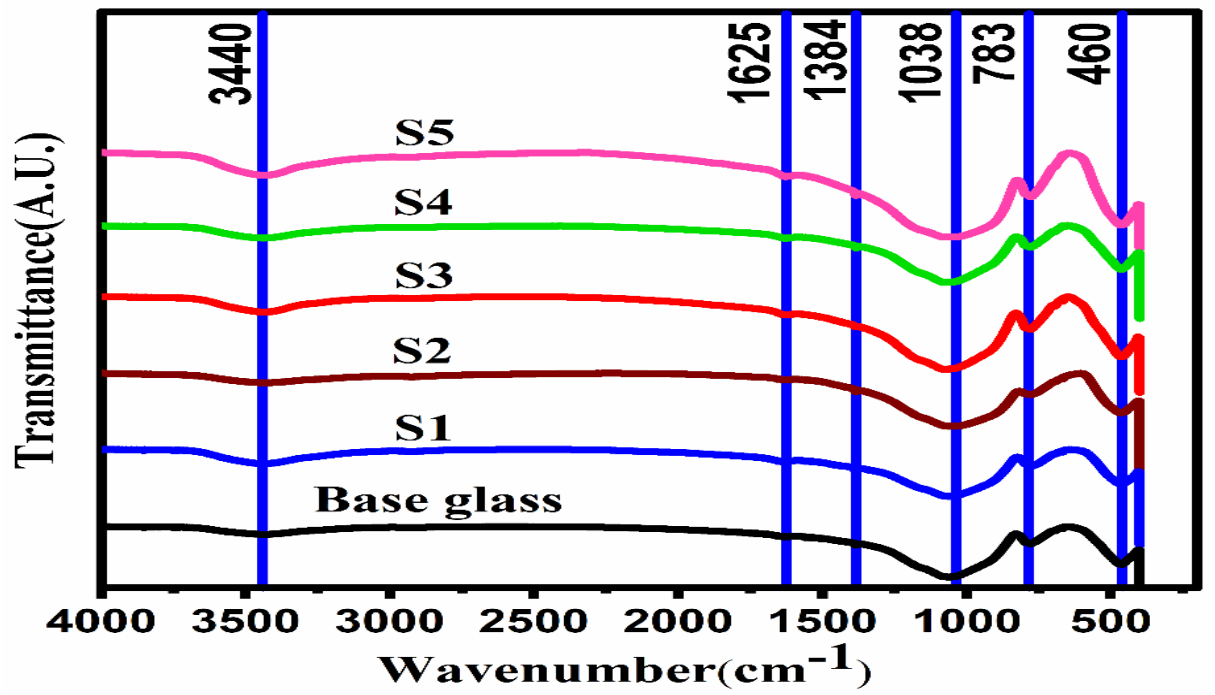

Fig. 4.4. FTIR spectra of all prepared glass samples with compositions xPbO-y(0.14Cu_2O-0.05CuO-0.03SnO_2)-30Na_2O-(70-0.22y-x)SiO_2, where (x, y) are (1.5, 0), (10, 0), (0, 1), (1.5, 1), and (10, 1) for samples S1, S2, S3, S4, and S5, respectively.

Likewise, glass samples S1, S2, S3, S4, and S5 exhibit the highest peak in the visible range at around 830 nm, 530 nm, 531 nm, 488 nm, and 491 nm, respectively, according to their obtained transparency (**Fig. 4.5(b)**).

4.3.4.1 *Visible Optical Properties*

The weighted mean of visible optical characteristics is computed using the following formulas, w hich are given below, and the reflectance, transmittance, and absorbance of chosen samples (S1, S2, S3, S4, & S5) covering the visible light wavelength of 360 nm to 830 nm are measured exper imentally using ISO standards [71].

$$T_{VIS} = \frac{\sum_{\lambda=360nm}^{\lambda=830nm} D_\lambda \tau(\lambda) v(\lambda) \Delta\lambda}{\sum_{\lambda=360nm}^{\lambda=830nm} D_\lambda v(\lambda) \Delta\lambda}$$

$$R_{VIS} = \frac{\sum_{\lambda=360nm}^{\lambda=830nm} D_\lambda \mu(\lambda) v(\lambda) \Delta\lambda}{\sum_{\lambda=360nm}^{\lambda=830nm} D_\lambda v(\lambda) \Delta\lambda}$$

The absorption from glass specimens over the visible region was provided by a correlation,

$$A_{VIS} = 100 - T_{VIS} - R_{VIS}$$

where $\Delta\lambda$ stands for wavelength intervals, D_λ is the relative spectral distribution of illuminate D65, $v(\lambda)$ is the spectral luminous efficiency for the field of view vision determining the average observer for spectrophotometric study, $\tau(\lambda)$ is spectral transmittance (%), and $\mu(\lambda)$ is spectral reflectance (%). **Table 4.4** lists all the visible optical characteristics that were measured for each glass sample using a UV-VIS spectrophotometer. When measuring daylighting in homes, the aforementioned observable features are crucial.

4.3.4.2 *Solar Optical Properties*

The following calculations, which use British and ISO standards, evaluate the solar optical properties of specific glass specimens in the entire visible spectrum wavelength range of 360 nm to 830 nm [**102**].

$$T_{solar} = \frac{\sum_{\lambda=360nm}^{\lambda=830nm} S_\lambda \tau(\lambda) \Delta\lambda}{\sum_{\lambda=360nm}^{\lambda=830nm} S_\lambda \Delta\lambda}$$

$$R_{solar} = \frac{\sum_{\lambda=360nm}^{\lambda=830nm} S_\lambda \mu(\lambda) \Delta\lambda}{\sum_{\lambda=360nm}^{\lambda=830nm} S_\lambda \Delta\lambda}$$

Whereas, solar absorbance is determined by the following relationship,

$$A_{solar} = 100 - T_{solar} - R_{solar}$$

S_λ is the relative spectral distribution of solar radiation (W/m^2). Building power consumption is increased by solar optical characteristics, which have a major effect on heating and cooling loads. These characteristics, which are listed in **Table 4.4**, are crucial for determining the heat load in homes across windowpanes.

Table 4.3. FTIR peak assignments for all prepared glass compositions.

Wavenumber (cm^{-1})	Bonding	Sources
460	**Bending vibrations of O-Si-O bonds in SiO_4 tetrahedral groups including oscillations of metal cations such as Pb^{2+}**	**[25,120]**
783	**Due to the bending of conjugated SiO_4 tetrahedral groups and oxygen atoms connected perpendicularly to the Si-Si axis within the Si-O-Si plane, in the SiO_2 glass network structure.**	**[120,121, 122]**
1038	**Uneven stretching of the O-Si-O bond within the SiO_4 tetrahedral group.**	**[63,119]**
1384	**Due to the antisymmetric vibrations of oxygen atoms connected to Si-O-Si groups**	**[119]**
1625	**Due to the vibration of the H_2O molecule and symmetric stretching of O-H bonds**	**[119,121]**
3440	**Associated with the stretching of the (OH) group and molecular water.**	**[70]**

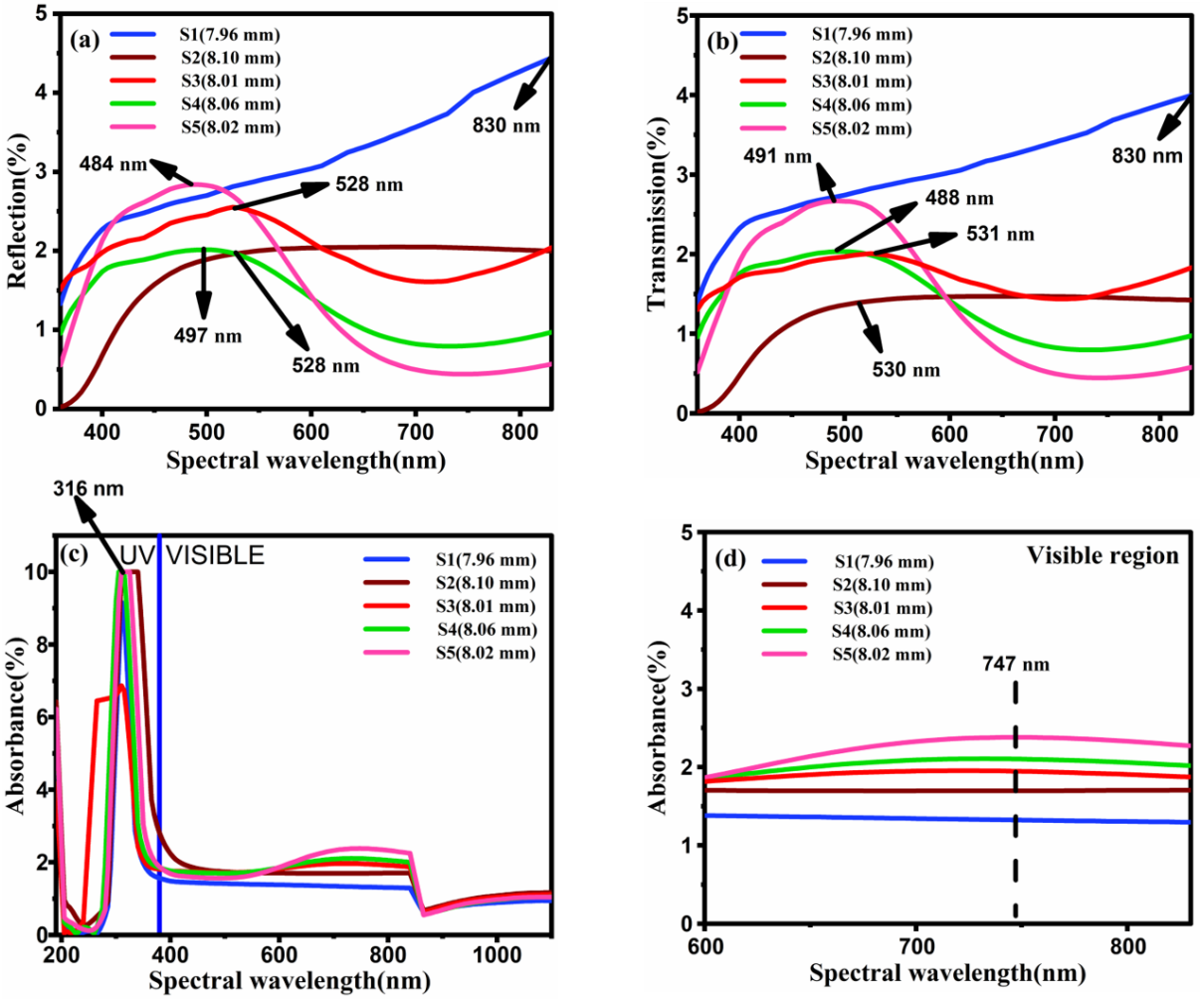

Fig. 4.5. Spectral reflections (a) in the visible range, spectral transmissions (b) in the visible range, spectral absorbance (c) in the UV and visible ranges, and spectral absorbance (d) in the 600 to 830 nm wavelength range within the visible region.

4.3.4.3 *Refractive index* (n) *and extinction coefficient* (k)

According to Fresnel's theory, which is given in the following formulas, the index of refraction (n), which is the real component of the complex refractive index, is related to the reflection function (R) and the extinction coefficient (k).

$$R = \frac{(n-1)^2 + k^2}{(n+1)^2 + k^2}$$

The refractive indices of complete synthetic glass specimens with different compositions are calculated using the algorithms listed in the following formulas.

Table 4.4. Visible and solar optical parameters, direct and indirect optical band gaps, and Urbach energy of all prepared glass samples.

Sample	Visible optical properties			Solar optical properties			E_{gind} (eV)	E_{gd} (eV)	E_U (eV)
	T_{VIS} (%)	R_{VIS} (%)	A_{VIS} (%)	T_{solar} (%)	R_{solar} (%)	A_{solar} (%)			
S1	40	40	20	40	41	19	2.61	3.03	0.0640
S2	27	38	35	27	37	36	2.42	2.86	0.0642
S3	31	39	30	30	36	34	1.90	2.80	0.0596
S4	33	32	35	28	28	44	1.85	2.60	0.0683
S5	34	36	30	28	29	43	1.64	2.57	0.0684

$$T_s = 10^{-A} \times 100$$

$$n = \frac{1}{T_s} + \sqrt{\frac{1}{(T_s - 1)}}$$

In this case, A stands for absorbance, and T_s for transmittance or transmittance constant. The following formula is used to calculate the extinction coefficient (k).

$$k = \frac{\alpha\lambda}{4\pi}$$

The absorption coefficient and wavelength of the materials are denoted by α and λ, respectively. Two major transmission factors that affect the refractive index of glass systems are connecting quasi-anions and cations in the ultraviolet region and grid oscillations in glass networking in the infrared region [8]. **Figs. 4.6** and **4.7** show the refractive index and extinction coefficient dispersion curves for the five prepared glass specimens. They show that the addition of the correspondingly determined amounts of metal oxides (Cu_2O+CuO+SnO_2) and PbO (**Table 4.1**) to the glass

composition improves the refractive index (n) and extinction coefficient (k) in the ultraviolet and visible regions.

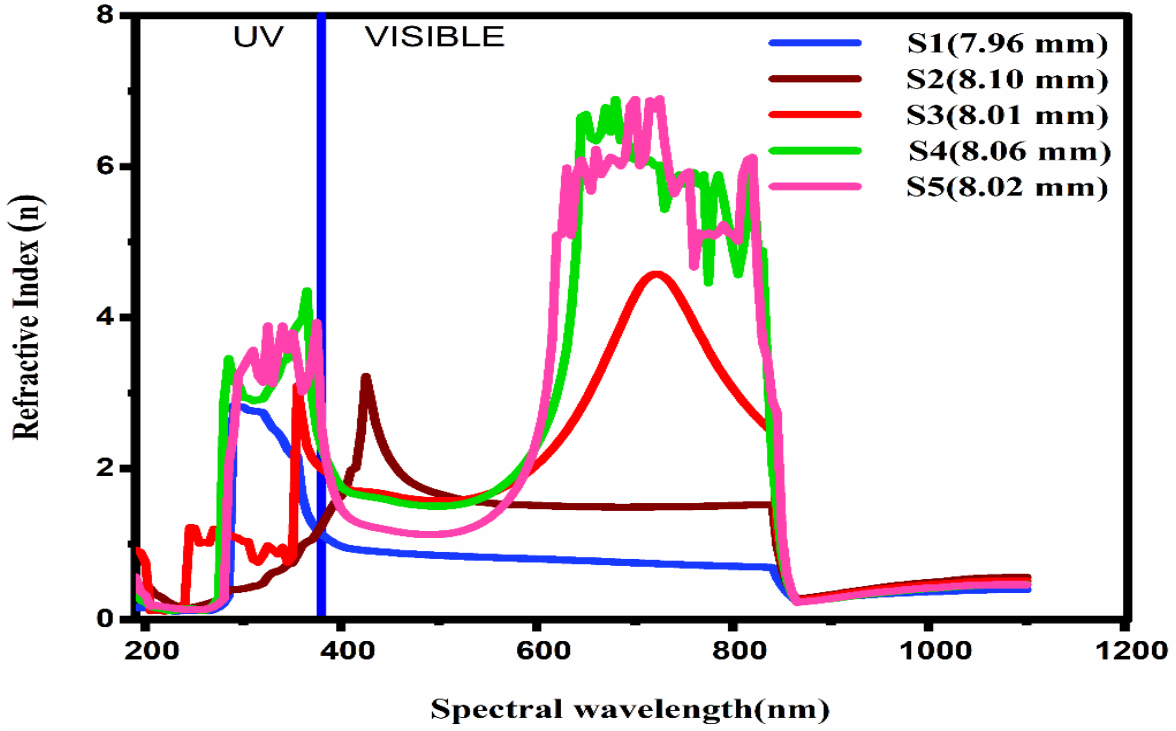

Fig. 4.6. Distribution plot of the refractive index (n) as a function of wavelength for all prepared glass samples.

4.3.4.4 *Complex dielectric constant*

The refractive index n and extinction coefficient k influence the optical complex dielectric const ant, which is established by molecular mechanisms resulting from photon interactions with electr ons. The real and imaginary components of the complex dielectric constants are denoted by $\mathcal{E}_r(\mathcal{E}_r = n^2 + k^2)$ and $\mathcal{E}_i(\mathcal{E}_i = 2nk)$ [8].

Fig. 4.8 shows the dispersion curves for the real component of the complex dielectric constant ($\mathcal{E}_r$) and the exponent of the complex dielectric constant ($\mathcal{E}_i$) of all five glass samples. It is clear from this that the addition of the correspondingly determined amount of metal oxides (**Table 4.1**) inside the sodium silicate glass structure causes both the real ($\mathcal{E}_r$) and imaginary ($\mathcal{E}_i$) components of the complex dielectric constant to develop highly within the ultraviolet and visible area.

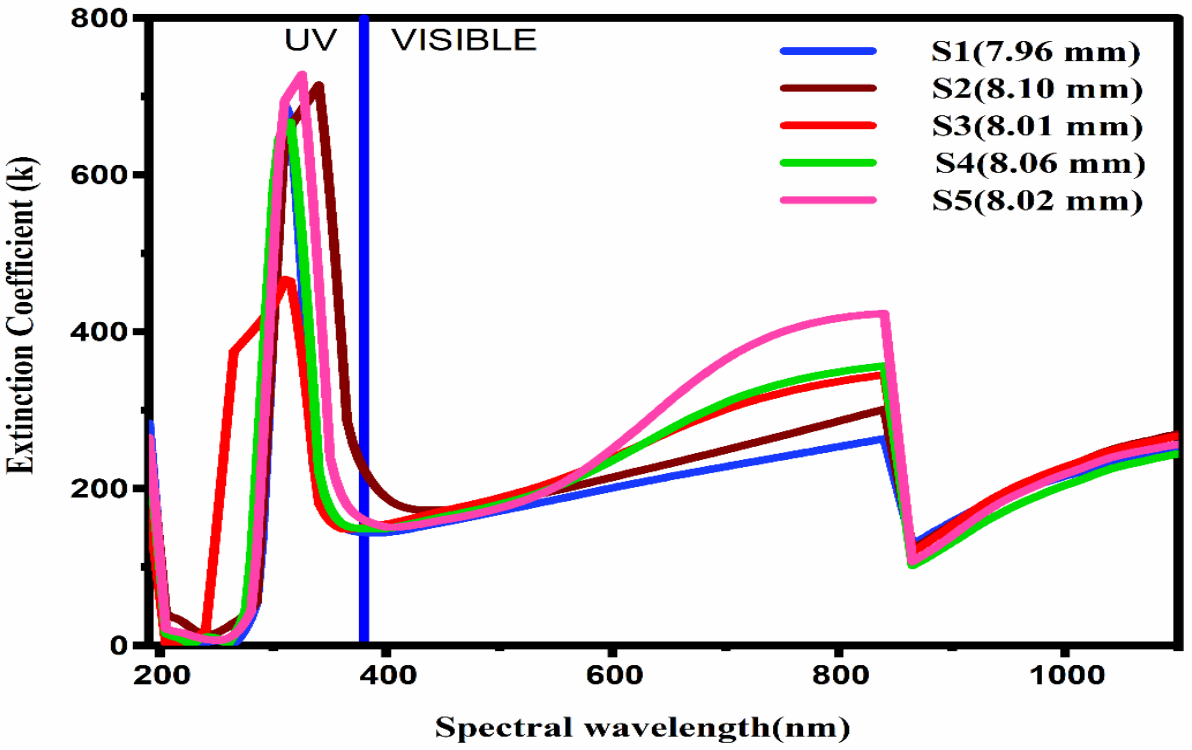

Fig. 4.7. Distribution plot of the extinction coefficient (k) versus wavelength for all prepared glass samples.

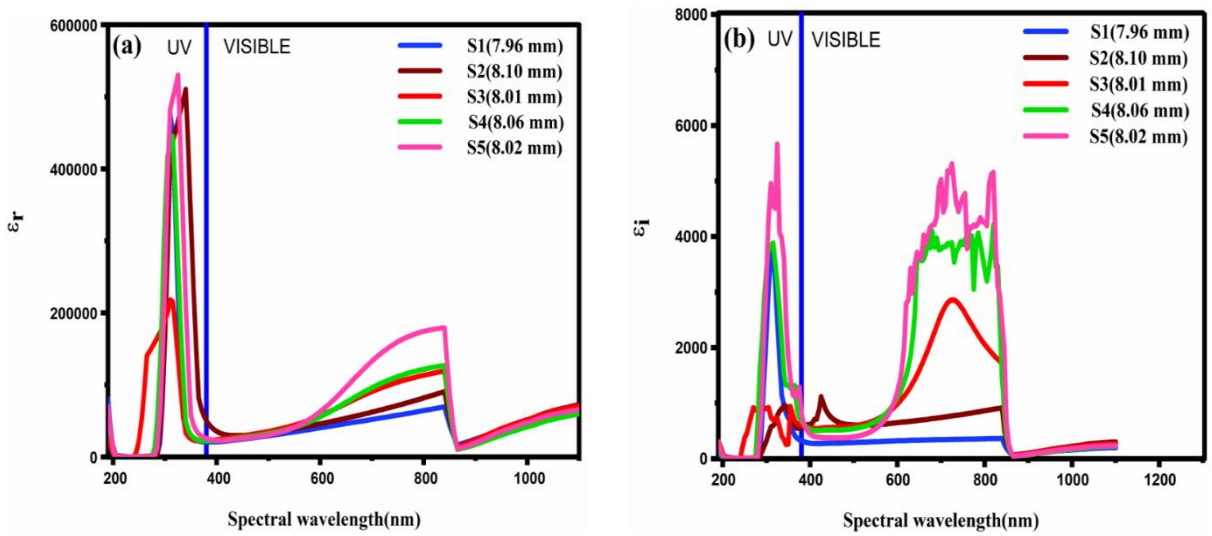

Fig. 4.8. Dispersion plot showing the real part of the complex dielectric constant ($\mathcal{E}_r$) and the imaginary part of the complex dielectric constant ($\mathcal{E}_i$) as a function of wavelength for the prepared glass samples.

4.3.4.5 *Evaluation of the Optical Band Gap*

For both indirect and direct transition, Tauc's plot of five comparable optically polished glass specimens with almost equivalent thicknesses but different compositions is shown in **Fig. 4.9** and **Fig. 4.10**, respectively. The energy gap of the synthesized samples is estimated using the Davis and Mott formula (Eq. (11)) [**8**].

$$(\alpha hv) = B\left(hv - E_g\right)^r$$

Where r is an index number with values of 1/2, 2, 3/2, and 1/3 according to the electronic transition pathway, B is a constant, E_g is an optical energy gap, and h is a plank constant. Permitted electronic transitions typically have r values of 1/2 for direct transitions and 2 for indirect transitions. To evaluate the optical band gap, the Tauc's plot between $(\alpha hv)^{1/r}$ on the ordinate and photon energy (hv) on the abscissa is built for each of the five glass samples with different compositions. By inferring the linear portion of Tauc's graph curve at $(\alpha hv)^r = 0$ (where r = 0.5 for indirect transition and r = 2 for direct transition), the optical band gaps are found. When the optical energy gap values of pure $30Na_2O$-$70SiO_2$ glass are taken from previous author research publications [**123**], the optical energy gap results for each of the five glass specimens are given in **Table 4.4**. The resulting optical energy gap (direct and indirect) of the y(1) glass series is significantly smaller than that of the y(0) glass series, as shown in **Fig. 4.11**. The addition of corresponding amounts of PbO (0≤x≤10, x in mol%) reduces the optical energy gap (direct and indirect) in both glass series.

4.3.4.6 *Assessment of molar refraction (R_m), polarizability (α_m), reflection loss (R_L), optical transmission (T), and metallization criterion (M_c) using the refractive index (n_0) derived from Tauc's method.*

The substance's molar refraction (R_m) determines the degree of total polarizability for each unit mole. The following Lorentz–Lorenz equation, is used to determine the molar refraction of a synthetic glass specimen [**104**].

$$R_m = \left(\frac{n_0^2 - 1}{n_0^2 + 2}\right) V_m$$

Where the refractive index (n_0) is determined using the following formula, and the obtained values are shown in **Table 4.5**. The (n_0) values (2.51-2.91) are considered significant and change as the concentration of PbO ($0 \leq x \leq 10$, x in mol%) in the glass system under study increases and the calculated amount of metallic concentration (<0.22mol%) (Cu_2O+CuO+SnO_2) is added.

$$\left(\frac{n_0^2 - 1}{n_0^2 + 2}\right) = 1 - \sqrt{\frac{E_g}{20}}$$

A molecule's electronic polarizability (α_m), which can be expressed as a function of molar refraction as used in the following formula, determines the amplitude of electrons interacting with an electric field.

$$\alpha_m = \left(\frac{R_m}{2.52}\right)$$

Consequently, the glasses in question can be used as promising candidates for various optical applications.

The following formulas were used to calculate the (R_L) and (T) values of the glass specimens that were made.

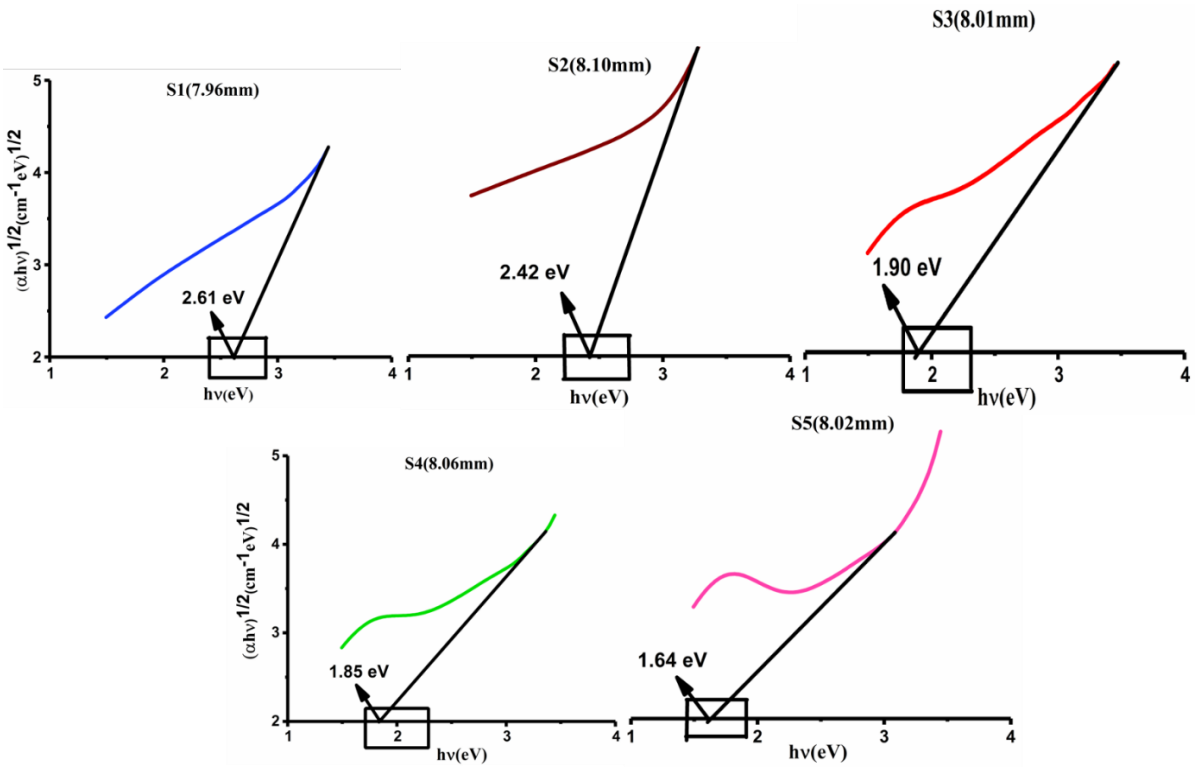

Fig. 4.9. The figure shows the Tauc's plot for the specified samples, indicating the indirect transitions.

$$R_L = \left(\frac{n_0 - 1}{n_0 + 1}\right)^2$$

$$T = \left(\frac{2n_0}{n_0^2 + 1}\right)$$

A material's status as an insulator or metallic is determined by its metallization criteria factor (M_c). The following formula is used to calculate the (M_c) values of complete synthesized glass specimens.

$$M_c = 1 - \left(\frac{R_m}{V_m}\right)$$

The bar graphs in **Figures 4.12(a)**, **4.12(b)**, **4.12(c)**, **4.12(d)**, and **4.12(e)** correspondingly show the (R_m), (α_m), (R_L), (T), and (M_c) values of the fully created glass specimens. We may conclude

that the prepared glasses are non-metallic (insulators) as the obtained (R_m) values of these created glasses are lower than their corresponding (V_m) values [104].

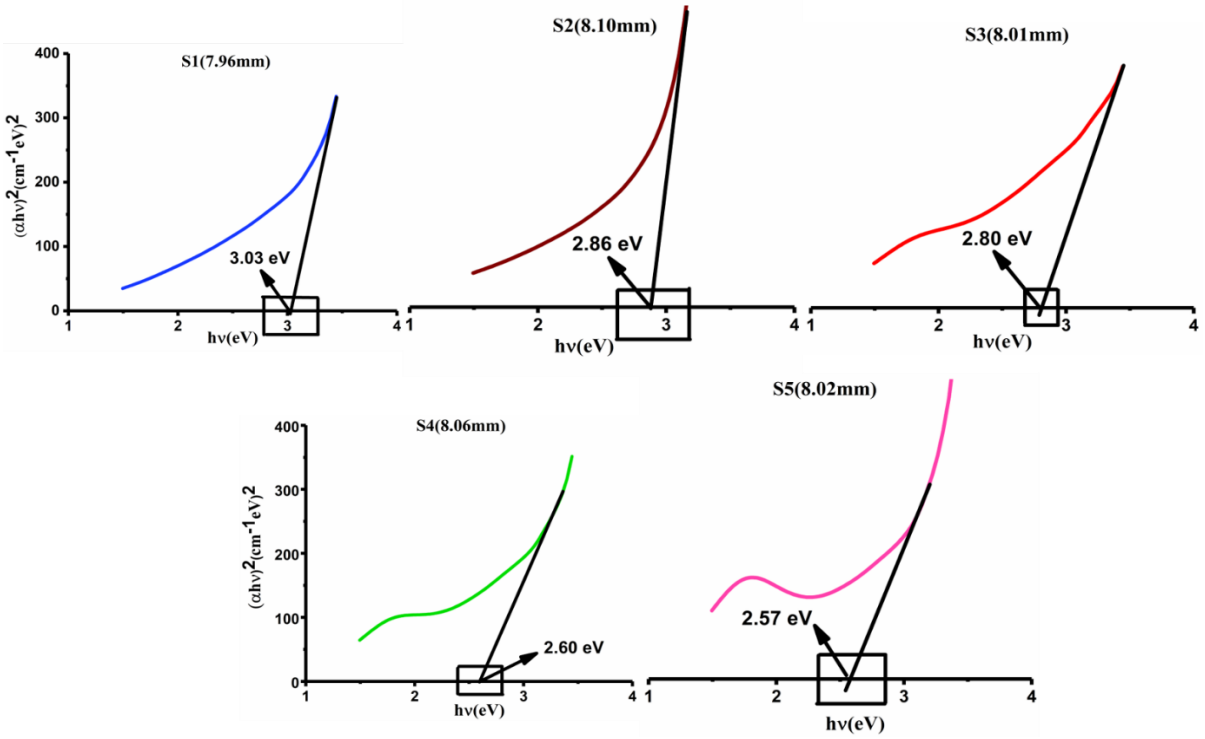

Fig. 4.10. The figure presents Tauc's plot for the specified samples, revealing direct transitions.

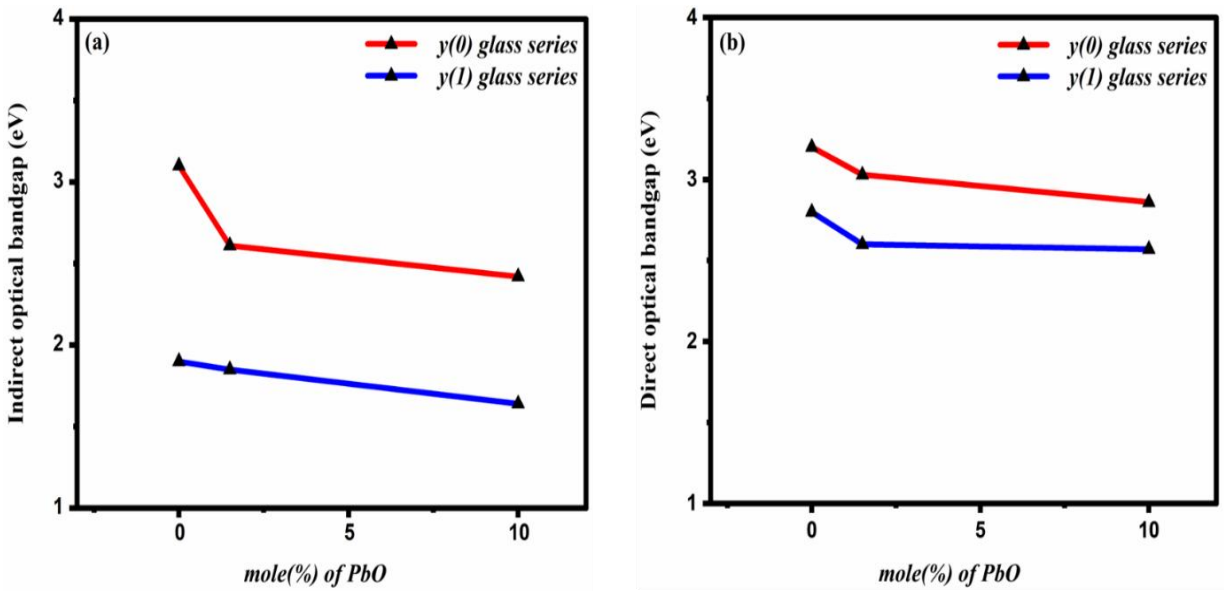

Fig. 4.11. The figure illustrates the effect of the addition of PbO ($0 \leq x \leq 10$, with x in mol%) on the indirect and direct optical energy gaps in the studied glass system {xPbO - y(0.14Cu_2O - 0.05CuO - 0.03SnO_2) - 30Na_2O - (70 - 0.22y - x) SiO_2}.

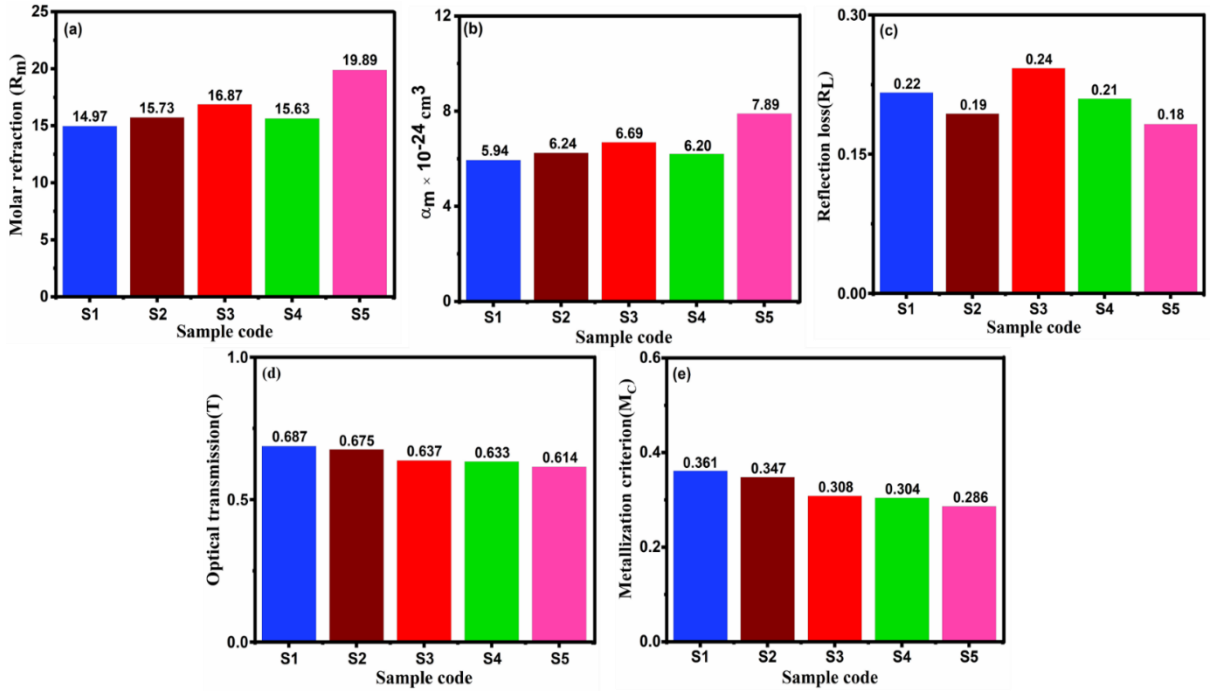

Fig. 4.12. The figure displays bar graphs for the studied samples, including the calculated molar refraction (R_m) in panel (a), polarizability (α_m) in panel (b), reflection loss (R_L in panel (c), optical transmission (T) in panel (d), and metallization criterion (M_c) in panel (e).

4.3.4.7 *Evaluation of optical electronegativity ($\Delta\chi^*$), third-order nonlinear optical susceptibility ($\chi^{(3)}$), and the corresponding nonlinear refractive index (n_2) using the refractive index (n_0) calculated via Tauc's method.*

The type of bonding in the samples is indicated by the optical electronegativity, ($\Delta\chi^*$) [124]. Ionic and covalent bonding is shown by the high and low ($\Delta\chi^*$) values, respectively. The formula below is used to calculate the (($\Delta\chi^*$) value of each prepared sample.

$$\Delta\chi^* = 0.2688\ (E_g)$$

The prepared specimens' bonding characteristic may be categorized as covalent bonding since the calculated ($\Delta\chi^*$) values are deemed weak, while the obtained values of ($\Delta\chi^*$) are depicted in the

bar graph of **Fig. 4.13(a)**. The resulting values $(\chi^{(3)})$ of the total analyzed glass specimens are shown in the bar graph of **Fig. 4.13(b)**, whereas the third-order nonlinear optical susceptibility $(\chi^{(3)})$ in the esu unit of the examined glasses is evaluated using the provided formula below. It is evident that the addition of a specific amount of metallic oxide (<0.22mol%) (Cu_2O+CuO+SnO_2) and the growing amount of PbO (0≤x≤10, x in mol%) concentration in the examined glass systems cause the $(\Delta\chi^*)$, & $(\chi^{(3)})$ values to decrease and increase, respectively.

$$\chi^{(3)}\ (\text{esu}) = \frac{A}{(4\pi)^4}\ (n_0^2 - 1)^4$$

Where A is fixed and roughly equals 1.7×10^{10}. All the chosen glasses' nonlinear refractive indices(n_2) are calculated using the subsequent formula and are shown in **Table 4.5**.

$$n_2(\text{esu}) = \frac{12\pi\chi^{(3)}}{n_0}$$

The results show that (n_2) changes when metallic oxides (<0.22mol%) (Cu_2O+CuO+SnO_2) and PbO (0≤x≤10, x in mol%) are added to the sodium silicate glass structure. This change is related to the amount of non-bridging oxygen (NBO) in the corresponding glass species.

Table 4.5. Calculated refractive index (n_0) adopting Tauc's method and, the corresponding nonlinear refractive index $(n_2) \times 10^{-13}$ for the studied glass specimens.

Sample code	**S1**	**S2**	**S3**	**S4**	**S5**
Calculated refractive index (n_0) via Tauc's method	**2.51**	**2.57**	**2.78**	**2.80**	**2.91**
Corresponding nonlinear refractive index $(n_2) \times 10^{-13}$ (esu)	**8.09**	**9.88**	**18.97**	**20.12**	**27.51**

4.3.4.8 *Determination of the Urbach Energy*

Urbach energy, which is only a little affected by temperature, has been used to measure energetic disorder at the band boundaries of semiconductors or insulators. In weak crystalline and chaotic amorphous materials, proximal states are formed as band ends in the traditional band gap and stretched in the band gap. In the poor photon energy domain, the absorption coefficient (α) is defined by the Urbach empirical rule as a function of photon energy (hv). The following formula presents the Urbach empirical rule.

$$\alpha = \alpha_0 \exp\left(\frac{hv}{E_U}\right)$$

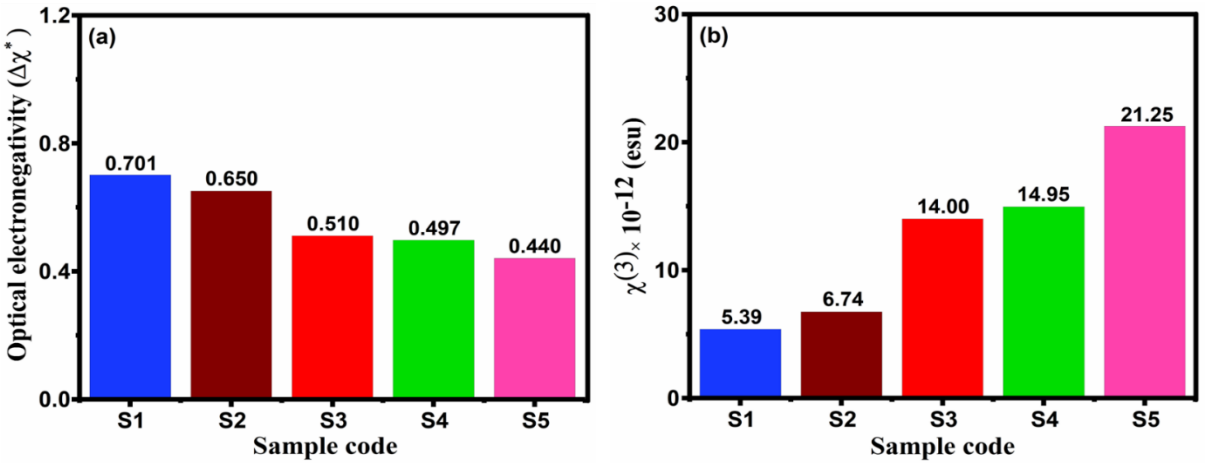

Fig. 4.13. The figure presents bar graphs for the studied samples, including the calculated optical electronegativity ($\Delta\chi^*$) in panel (a) and the third-order nonlinear optical susceptibility $\left(\chi^{(3)}\right)$ in panel (b).

The constant and band tail energy, or Urbach energy, are represented by α_0 and E_U, respectively. Considering the logarithms of the two sides of the Urbach empirical equation above, we get at

$$\ln(\alpha) = \ln(\alpha_0) + \left(\frac{hv}{E_U}\right)$$

By plotting $\ln(\alpha)$ against incident photon energy (hv), we obtain $E_U = \frac{1}{m}$, where m is the gradient of a straight line. To determine each specimen's Urbach energy, **Fig. 4.14** shows the graph of $\ln(\alpha)$ vs. incoming photon energy (hv) of prepared samples with different compositions. For the glass

specimens used in the study, the Urbach value varies from 0.0596 to 0.0684 eV (**Table 4.4**). The Urbach energy increases when the glass's metallic concentrations (<10.22 mol%) (Cu_2O+CuO+SnO_2+ PbO) increase, suggesting that the concentrations of defects in the glass matrix also increase.

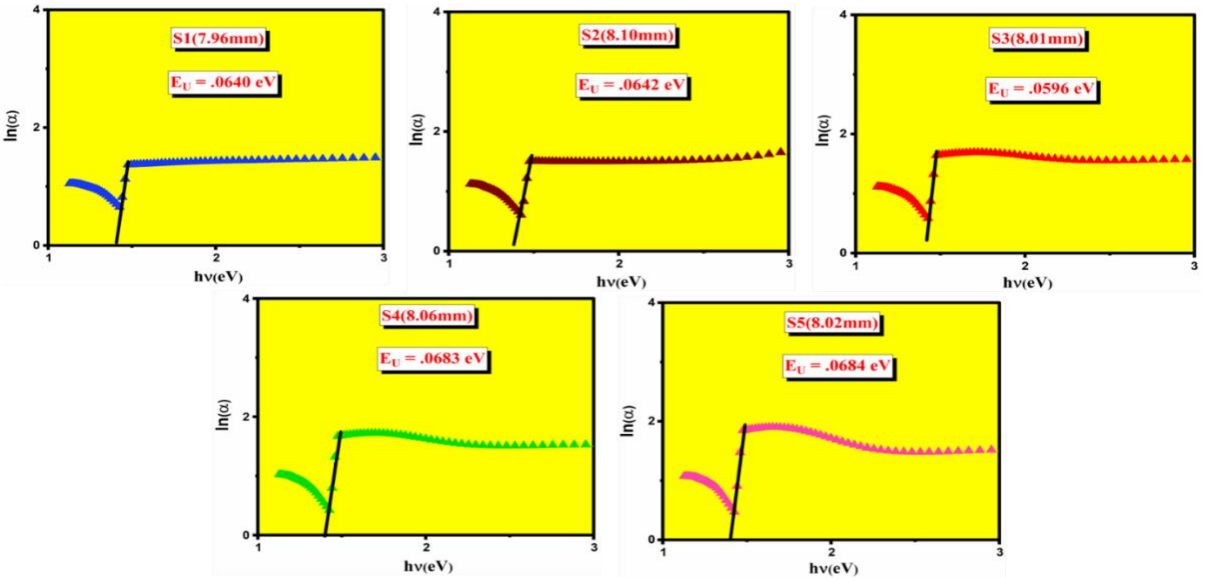

Fig. 4.14. Graph of ln(α) versus incident photon energy (hv) for the examined specimens.

4.3.4.9 ***Examination of UV-Vis Absorption Edges***

The composition of the parent glass, melting temperature, duration of the melting process, partial pressure of oxygen during melting, annealing temperature, rate of cooling, and background losses (reflection loss, absorbance caused by OH groups, IR edge, etc.) detected in the absorbance spectra due to dopants, refining compounds, and other absorbent impurities are the main factors influencing the absorbance spectrum of prepared glass samples [**72**]. All the glass specimens exhibit a maximum absorbance of approximately 316 nm in the UV region (**Fig. 4.5(c)**). In contrast, the absorption assessment of the primarily metallic doped glass specimens (S3, S4, S5) reveals a maximum absorbance of approximately 747 nm in the visible area (**Fig. 4.5(d)**). The metallic element copper appears as Cu^{2+} ions in the already manufactured glass samples (S3, S4,

S5) at typical melting conditions, but part of it exists as Cu^0 and Cu_2O [**75-78**]. In silicate glasses, the absorption band resulting from Cu^{2+} ions was previously detected at 786 nm, in alumina-boro-phosphate glasses at 1048 nm, and in sodium alumina-borate glasses at 1390 nm [**15**,**74**, **79**, **80**, **81**]. A developing single broad absorption band from 600 nm to 830 nm is seen in the currently made glass samples (S3, S4, S5) including Cu_2O, and CuO (**Fig. 4.5(d)**). This band is most likely associated with the assignment of an electronic transition of one of the ingredient's cupric ions. The electronic transition from the $^2E_g \rightarrow {}^2T_g$ energy level in the octahedral coordination of the Cu^{2+} ion may be the source of the detected rising band, suggesting a distorted octahedral symmetry for cupric ions in the present S3, S4, and S5 glass samples [**81**,**82**]. The all-glass samples (S1, S2, S3, S4, S5) show a significant charge transfer ultraviolet absorption band at about 316 nm, which could be due to the presence of Pb^{2+} ions in the all-respective glass samples as well as iron impurities [**125**].

4.3.5 *Optical Basicity of Tinted Glasses (Λ_{th})*

The optical basicity parameter (Λ) indicates the ability of oxide glasses to generate a negative charge to the probing ion and can be used to classify a variety of oxidic glasses based on their basicity order [**13**, **65**]. It links properties such as refractive index without reference to the glass's anionic structure [**65**]. Glass's optical basicity might be predicted based on its composition, according to Duffy and Ingram, who also suggested the following method to calculate this parameter [**13**].

$$\Lambda_{th} = \sum_{i} X_i \Lambda_i$$

Where Λ_i is the basicity ascribed to the corresponding oxide and X_i is the equivalent fraction derived from the amount of oxygen supplied by each oxide to the overall glass stoichiometry [**126**, **127**]. The following formula is used to calculate the basicity moderating parameter (γ_i) [**128**].

$$\gamma_i = 1.36(x_i - 26)$$

Where x_i is the Pauling electronegativity of the cation. The bar graph in **Fig. 4.15** is used to analyze and report the optical basicity (Λ_{th}) of the created glasses. **Table 4.6** below lists all the cations that are present in the glass matrices along with their optical basicity (Λ), Pauling electronegativity (x_i), and optical basicity moderating parameter (γ_i). As the addition of metallic oxides (<0.22 mol%) (Cu_2O+CuO+SnO_2) and PbO ($0 \leq x \leq 10$, x in mol%) increases due to expanding electrons on oxygen atoms, the optical basicity (Λ_{th}) readings increase from 0.5986 to 0.6508 [**127**].

4.3.6 *Mechanical properties*

The measured longitudinal ultrasonic velocity (V_L) and shear ultrasonic velocity (V_S) were used to calculate the longitudinal (L_m), shear (G_m), bulk (k_m), Young's (E_m) modulus, hardness (H), and Poisson's ratio (υ) of the corresponding tint glasses. The corresponding values are provided in **Table 4.7** [**129**]. The following lists the formulas used to calculate the mechanical characteristics.

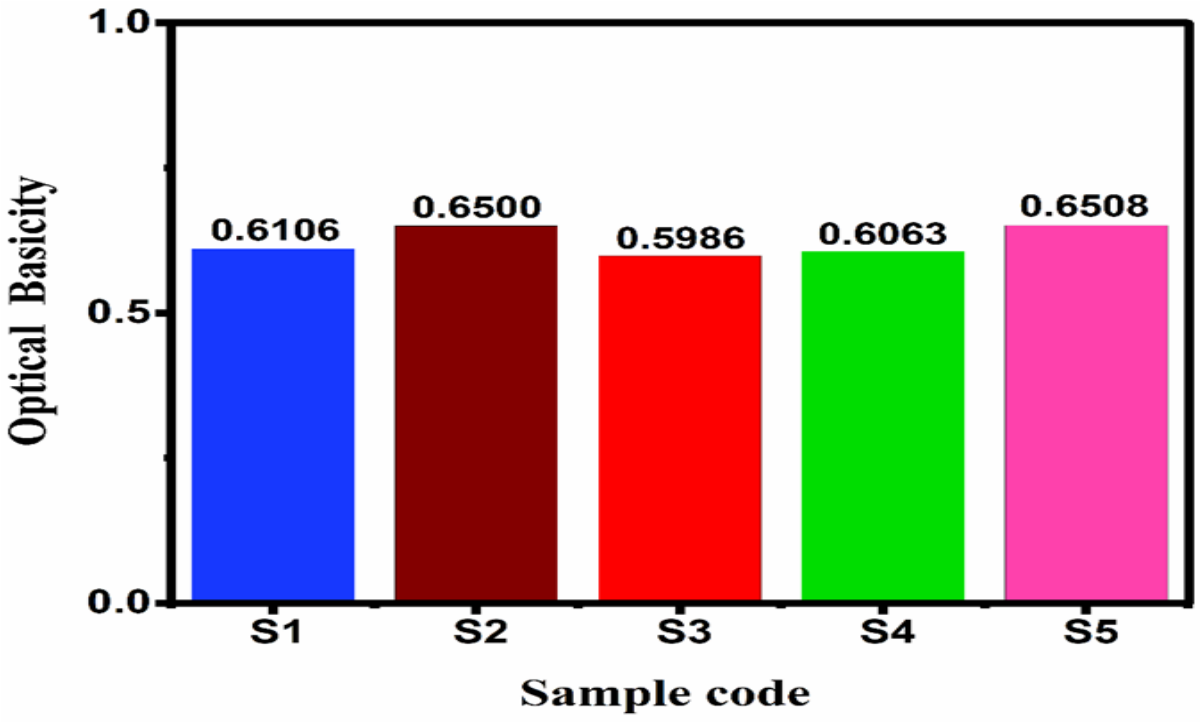

Fig. 4.15. Bar chart of the analysed samples showing the calculated optical basicity.

Table 4.6. Basicity Properties of Glasses.

Cation	Pauling electronegativity (x_i)	Basicity moderating parameter (γ_i)	$(\Lambda) = \frac{0.75}{(x_i - 0.25)}$	$(\Lambda) = [\gamma_i]^{-1}$
Pb	**2.33**	**2.8152**	**0.360576923**	**0.35521455**
Na	**0.93**	**0.9112**	**1.102941176**	**1.097453907**
Si	**1.9**	**2.2304**	**0.454545455**	**0.448350072**
Cu	**1.9**	**2.2304**	**0.454545455**	**0.448350072**
Sn	**1.96**	**2.312**	**0.438596491**	**0.432525952**

$$L_m = \rho V_L^2$$

$$G_m = \rho V_s^2$$

$$k_m = L_m - \left(\frac{4}{3}\right) G_m$$

$$E_m = \frac{9 k_m G_m}{3 k_m + G_m}$$

$$H = \frac{(1 - 2\upsilon) E_m}{6(1 + \upsilon)}$$

Table 4.7. Mechanical Properties of Tinted Glasses.

Samples	V_L (m/s)	V_S (m/s)	L_m (GPa)	G_m (GPa)	k_m (Gpa)	E_m (Gpa)	H (GPa)	υ
S1	**5954.77**	**3609.83**	**95.35**	**35.04**	**48.63**	**84.76**	**6.78**	**0.2095**
S2	**5134.98**	**3200.22**	**84.11**	**32.67**	**40.55**	**77.26**	**6.91**	**0.1824**
S3	**6118.72**	**3761.77**	**93.26**	**35.25**	**46.26**	**84.33**	**7.14**	**0.1962**
S4	**6274.08**	**3805.79**	**101.78**	**37.45**	**51.84**	**90.54**	**7.26**	**0.2089**
S5	**5447.76**	**3296.12**	**82.06**	**30.04**	**42.00**	**72.77**	**5.78**	**0.2113**
Base glass	**6091.32**	**3738.36**	**89.05**	**33.54**	**44.33**	**80.35**	**6.75**	**0.1978**

$$\upsilon = \frac{E_m}{2G_m} - 1$$

By using the Makishima and Mackenzie model [130], the mechanical properties of the synthesized glasses have also been examined. These qualities depend on the chemical composition, packing density (V_t), and dissociation energy per unit volume (G_t) of the individual glasses. Using the following formulas, the mechanical properties of the glasses were calculated according to the MM model: Young's (E_m), bulk (k_m), shear (G_m), longitudinal (L_m) modulus, Poisson's ratio (υ), fractal bond connectivity (d_f), and hardness (H). The corresponding mechanical properties are displayed in **Table 4.8**.

$$V_t = \left(\frac{1}{V_m}\right)\sum y_i V_i$$

$$V_i = N_A\left(\frac{4\pi}{3}\right)(xR_A^3 + yR_O^3)$$

In an oxide, A_xO_y system, where R_A and R_O represent the Pauling ionic radii of cation and oxygen, respectively, and N_A and y_i represent Avogadro's number and mole fraction of component i, respectively.

$$E_m = 2V_tG_t$$

$$k_m = 10V_t^2G_t$$

$$G_m = \frac{30V_t^2G_t}{(10.2V_t - 1)}$$

$$L_m = k_m + \left(\frac{4}{3}\right)G_m$$

$$\upsilon = 0.5 - \left(\frac{1}{7.2V_t}\right)$$

$$d_f = 4 \times \left(\frac{G_m}{k_m}\right)$$

$$H = \frac{(1-2\upsilon)E_m}{6(1+\upsilon)}$$

The packing density parameter in the Makishima and Mackenzie model has been updated as in the bellow formulas and is displayed in **Table 4.9**; the all-similar mechanical parameters have also been calculated by the Rocherulle model.

$$C_t = \sum_i y_i C_i$$

$$C_i = N_A \left(\frac{4\pi}{3V_m}\right)(xR_A^3 + yR_O^3)$$

The microstructure of the glass samples under study is represented by the fractal bond connectivity (d_f), which ranges from 3.00 to 2.40 [**129**]. For chain, layer structure, and 3D networks of tetrahedral coordination polyhedral systems, the (d_f) value changes to 1, 2, and 3, respectively. A 3D layer glass network structure is implied by the fact that the obtained (d_f) values of the examined glass specimens are extremely like 3.

Table 4.8. Mechanical Properties of the Glasses Based on the Makishima & Mackenzie Model.

Samples	V_t	$G_t \times 10^6$ (KJ/m^3)	E_m(Gpa)	k_m(Gpa)	G_m(Gpa)	L_m(Gpa)	υ	d_f	H (Gpa)
S1	**0.5598**	**58.14**	**64.90**	**43.37**	**27.54**	**80.17**	**0.2518**	**2.54**	**4.2893**
S2	**0.5362**	**54.52**	**58.34**	**37.45**	**25.35**	**71.54**	**0.2409**	**2.70**	**4.0604**
S3	**0.5393**	**58.76**	**63.49**	**40.88**	**27.98**	**78.36**	**0.2424**	**2.74**	**4.3880**
S4	**0.5838**	**58.11**	**67.72**	**47.29**	**28.42**	**85.24**	**0.2621**	**2.40**	**4.2549**
S5	**0.4636**	**54.48**	**50.39**	**30.04**	**22.54**	**60.17**	**0.2000**	**3.00**	**4.1991**
Base glass	**0.5211**	**58.79**	**61.39**	**38.67**	**26.56**	**74.12**	**0.2334**	**2.75**	**4.4231**

As the concentrations of PbO ($0 \leq x \leq 10$, x in mol%) in the pure sodium silicate glass network structure and the calculated number of metallic oxides ($Cu_2O+CuO+SnO_2$) (<0.22mol%) added to the sodium silicate glass structure increase, respectively, the mechanical properties of the examined glass specimens are reduced (**Fig. 4.16**). The features in **Fig. 4.16** further demonstrate that the addition of metallic oxides ($Cu_2O+CuO+SnO_2$) (<0.22 mol%) in the sodium silicate glass networks has significantly enhanced the properties of the y(1) glass series compared to the y(0) glass series. As PbO concentrations increase ($0 \leq x \leq 10$, x i

Table 4.9. Mechanical Properties of the Glasses Determined Using the Rocherulle Model.

Samples	$\mathbf{C_t}$	$\mathbf{G_t^* \times 10^6}$ **(KJ/m^3)**	$\mathbf{E_m^*}$ **(Gpa)**	$\mathbf{k_m^*}$**(Gpa)**	$\mathbf{G_m^*}$**(Gpa)**	$\mathbf{L_m^*}$**(Gpa)**	$\boldsymbol{\upsilon^*}$	$\mathbf{d_f^*}$	$\mathbf{H^*}$**(Gpa)**
S1	0.5503	58.14	64.02	42.18	27.56	78.53	0.2476	2.61	4.317
S2	0.5404	54.52	58.93	38.15	25.36	72.04	0.2429	2.66	4.063
S3	0.5519	58.76	64.87	42.56	27.54	79.35	0.2483	2.59	4.360
S4	0.5502	58.11	63.86	42.05	27.34	78.64	0.2475	2.60	4.309
S5	0.5402	54.48	58.76	38.00	25.28	71.56	0.2428	2.66	4.053
Base glass	0.5521	58.79	64.84	42.56	27.64	79.56	0.2484	2.59	4.356

mol%), the mechanical characteristics of both glass series (y (1) and y (0)) decline because the packing density (V_t) and dissociation energy (G_t) of the glass specimens under study diminish. As the PbO mol% increases, the molar volume (V_m) (cm^3) of the glass samples under study increases, resulting in a decrease in the packing density, (V_t). Similarly, when the PbO (mol%) concentrations increased in the glass latticework, the dissociation energy of the glasses decreased because the bond force of Pb-O was lower than that of Si-O. Therefore, when PbO mol% increases,

the stiffness of the glass samples under study, including their total modulus of elasticity, decreases because the values of V_t and G_t fall. This is followed by an increase in molar volume (V_m) (cm^3).

4.4 Conclusions

Throughout the study, two distinct sodium silicate glass series were successfully synthesized using the melt annealing method: the first (y(0)) was doped solely with PbO, while the second (y(1)) was doped with Cu_2O, CuO, SnO_2, and PbO in varying ratios. The amorphous character of the samples is confirmed by the X-ray diffraction examination, which reveals no non-crystallographic peaks. UV-Visible spectroscopy is used to perform reflection, transmission, and absorption examinations of the corresponding specimens. It has also proven helpful in determining the optical band gap energy of the specimens. The measured indirect

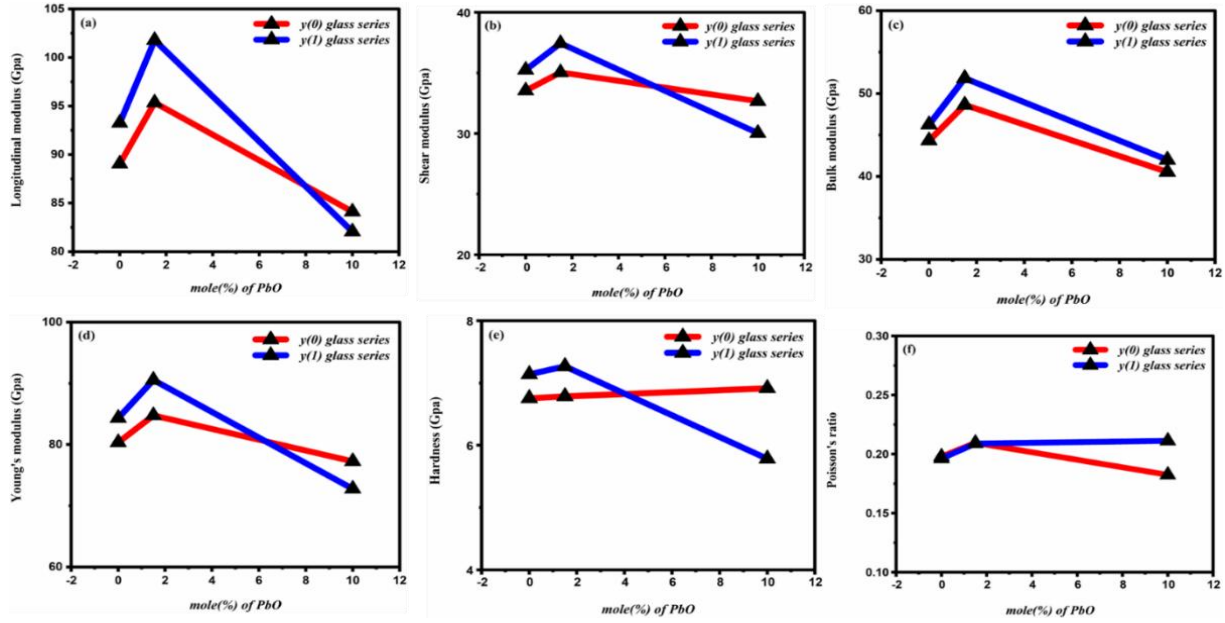

Fig. 4.16. Effect of PbO Addition ($0 \leq x \leq 10$, x in mol%) on the Mechanical Properties of the Investigated Glass System {xPbO - y(0.14Cu_2O - 0.05CuO - 0.03SnO_2) - 30Na_2O - (70 - 0.22y - x) SiO_2}.

energy gap (E_{gind}) of the examined samples ranges from 1.64 to 2.61 eV. Until metallic oxides (Cu_2O+CuO+SnO_2+PbO) are added to sodium silicate glass networks at a maximum of 10.22 mol%, the resulting glass series are found to be translucent. In the studied samples, the parameters that control daylighting in the building, such as R_{VIS} , T_{VIS} , and A_{VIS} , were found to

be between 32 and 40%, 27 and 40%, and 20 and 35%, respectively. The parameters that measure the building's heat gain, such as R_{solar} , T_{solar} , and A_{solar}, were found to be between 28 and 41%, 27 and 40%, and 19 and 44%, respectively. Additionally, it is shown that the refractive index (n), extinction coefficient (k), and complex dielectric constants ($\mathcal{E}_r$, $\mathcal{E}_i$) of the synthesized specimen glasses are improved by the addition of PbO ($0 \leq x \leq 10$, x in mol%) and metallic oxides ($Cu_2O+CuO+SnO_2$) (<0.22 mol%) in sodium silicate glass networks. Pb^{2+} ions and the presence of Fe^{3+} ions as an impurity caused the significant charge transfer UV absorption band, which is visible at about 316 nm for all the glass specimens under study. Each evaluated glass specimen's average refractive index (n_0) and corresponding nonlinear refractive index (n_2) are determined using Tauc's approach; the values of (n_0) range from 2.51 to 2.91. In addition, the following parameters have been computed for the examined glass specimens: oxygen packing density, optical basicity (Λ_{th}), molar refraction (R_m), polarizability (α_m), reflection loss (R_L), optical transmission (T), metallization criterion (M_c), optical electronegativity ($\Delta\chi^*$), and third-order nonlinear optical susceptibility ($\chi^{(3)}$). The results of every characteristic show that the addition of metallic oxides ($Cu_2O+CuO+SnO_2$) (<0.22 mol%) and PbO mol% concentrations is closely linked to the optical and physical properties of all glasses under study. When PbO concentrations were gradually added, the elastic moduli and rigidity of the $xPbO\text{-}y(0.14Cu_2O\text{-}0.05CuO\text{-}0.03SnO_2)\text{-}30Na_2O\text{-}(70\text{-}0.22y\text{-}x)\ SiO_2$ glass systems decreased. As PbO concentrations in the glasses increase, the packing density (V_t) and dissociation energy (G_t) of the glasses under study drop, resulting in a fall in the stated mechanical parameters. In contrast to improving absorption, refractive index, and density, increasing metallic concentrations significantly reduces mechanical and visual properties like transparency, producing unsightly black, darker glasses. Therefore, it appears that the goal of this study is to determine the ideal concentration of metals in sodium silicate glass structures to produce exceptional dense optical glasses with exceptional mechanical qualities, refractive index, and transparency that may prove to be very helpful when used as building materials and optoelectronic tools in the not-so-distant future.